Available online at www.sciencedirect.com

ScienceDirect

Ceramics International 40 (2014) 2477–2481

CERAMICS INTERNATIONAL

www.elsevier.com/locate/ceramint

Short communication

Microstructure and varistor properties of Y_2O_3-doped ZnO–Pr_6O_{11}–CoO–Cr_2O_3–La_2O_3 ceramics

Choon–W. Nahm*

Semiconductor Ceramics Laboratory, Department of Electrical Engineering, Dongeui University, Busan 614-714, Republic of Korea

Received 25 May 2013; accepted 1 July 2013
Available online 6 July 2013

Abstract

The microstructure, electrical properties, and aging behavior of Y_2O_3–doped ZnO–Pr_6O_{11}–CoO–Cr_2O_3–La_2O_3 varistor ceramics have been systematically investigated for different amounts of Y_2O_3. As the amount of Y_2O_3 increased, the sintered density increased from 4.97. 5.18, and 5.20 g/cm^3 and the average grain size decreased from 4.1, 3.9, and 3.7 μm. The breakdown field increased from 8953 to 9731 V/cm with an increase in the amount of Y_2O_3. The varistor ceramics doped with 0.5 mol% in the amount of Y_2O_3 exhibited the highest nonlinear coefficient of 60.9. The varistor ceramics doped with 1.0 mol% in the amount of Y_2O_3 exhibited a surprisingly excellent stability by exhibiting –0.5% in the variation rate of the breakdown field and 2.5% in the variation rate of the nonlinear coefficient for aging stress of 0.95 E_B/150 °C/24 h.

Keywords: B. Grain boundaries; C. Electrical properties; C. Aging behavior; D. ZnO; E. Varistors

1. Introduction

Advanced electronic components are featured by miniaturization with lightweight, thin-film, short-length, and small size. Furthermore, functionally, they are featured by low voltage, low power loss, high speed, etc. This is heavily indebted to the development of semiconductor devices. To operate normally electronic system, the semiconductor devices very susceptible to transient overvoltage should be protected under any situation. One of many countermeasures for transient overvoltage is to use a varistor.

ZnO varistors are electroceramic devices made by sintering ZnO powder added with minor impurities [1,2]. The ceramic varistors have a distinctive microstructure composed of a lot of grains and multi-junctions which are distributed 3-dimensionally through entire sintered ceramics [1,2]. When the junctions at grain boundaries are active, the ZnO varistors have electrical function, which exhibit nonlinear voltage–current characteristics. This is similar to the back-to-back zener diode, whereas this has much stronger absorption capability against transient overvoltage than that of zener diode [1,2].

The majority of commercial ZnO varistor ceramics are added with Bi_2O_3 as varistor forming oxides. They have been extensively used in electronic system, electrical apparatus and facility based on excellent nonlinear properties. However, they have the high volatility of Bi_2O_3 itself and active reactivity with other additives caused by low melting point (825 °C) of Bi_2O_3 [3]. To solve these problems, Pr_6O_{11}-doped ZnO varistor ceramics have been studying as new alternative varistors replacing ZnO–Bi_2O_3 varistor ceramics [4–10]. The rare earth oxide-doped ZnO–Pr_6O_{11} varistor ceramics were reported to have good nonlinear properties and strong stability against a stress [8,11–17]. These varistor ceramics are limited to five components. To develop varistor ceramics having higher performance and diverse applications, it is necessary to scrutinize the effects of additives and sintering process on varistor properties and aging behavior against a stress. The objective of this work is to systematically explore microstructure, nonlinear electrical properties, and aging behavior of Y_2O_3-doped ZnO–Pr_6O_{11}–CoO–Cr_2O_3–La_2O_3 varistor ceramics with 6-components [17–19]. New experimental results were that these varistor ceramics exhibited excellent nonlinear properties and stronger stability against a severe stress state.

*Tel.: +82 51 890 1669; fax +82 51 890 1664.
E-mail address: cwnahm@deu.ac.kr

0272-8842/$ - see front matter © 2013 Elsevier Ltd and Techna Group S.r.l. All rights reserved.
http://dx.doi.org/10.1016/j.ceramint.2013.07.007

2. Experimental procedure

The raw materials for the ceramic composition are follows: (97.75-x) mol% ZnO, 0.5 mol% Pr_6O_{11}, 1.0 mol% CoO, 0.5 mol% Cr_2O_3, 0.25 mol% La_2O_3, x mol% Y_2O_3 (x=0.25, 0.5, 1.0). All the powders were mixed by ball milling with zirconia balls and acetone in a polypropylene bottle for 24 h. The mixture calcined in air at 750 °C for 2 h was granulated by sieving through a 100-mesh screen to produce the starting powder after the addition of 2 wt% polyvinyl alcohol (PVA) binder. The powders were pressed into disk-shaped pellets of 10 mm in diameter and 2 mm in thickness at a pressure of 80 MPa. The pellets were sintered at 1300 °C in air for 1 h. The sintered pellets were lapped and polished to 1.0 mm thickness. The final pellets were about 8 mm in diameter and 1.0 mm in thickness. Silver paste was coated on both surfaces of the pellets to serve as electrodes, and the electrodes were formed by heating it at 600 °C for 10 min. Finally, after soldering the lead wire to both electrodes, the samples were packaged by dipping them into a thermoplastic resin powder.

The surface microstructure was examined by a scanning electron microscope (SEM, Hitachi S2400; Chiyoda-Ku, Tokyo, Japan). The average grain size (d) was determined by the lineal intercept method, given by d=1.56L/MN, where L is the random line length on the micrograph, M is the magnification of the micrograph, and N is the number of grain boundaries intercepted by the lines [20]. The crystalline phases were identified using an X-ray diffractometer (XRD, Rigaku D/max 2100; Shibuya-Ku, Tokyo, Japan) using a CuK_α radiation. The densities (ρ) sintered pellets were measured using a programmable density determination kit (238490) attached to a balance (Mettler Toledo AG 245, Mettler Toledo International Inc., Greifensee, Switzerland), with deionized water as a liquid medium.

The electric field–current density (E–J) characteristics were measured using a high voltage source-measure unit (Keithley 237; Keithley Instruments Inc., Cleveland, OH, USA). The breakdown field (E_B) was determined at 1.0 mA/cm^2 in the leakage current density and the leakage current density (J_L) was determined at 0.8 E_B. In addition, the nonlinear coefficient (α) is defined by the empirical law, $J=C\cdot E^{\alpha}$, where J is the current density, E is the applied electric field, and C is a constant. The α was calculated in the current density range of 1.0 mA/cm^2–10 mA/cm^2 from the following expression: $\alpha=1/(\log E_2-\log E_1)$, and E_1 and E_2 are the electric fields corresponding to 1.0 mA/cm^2 and 10 mA/cm^2, respectively.

The DC-accelerated aging stress test was performed under four continuous conditions as follows: the 1st stress: 0.85 E_B/115 °C/24 h, the 2nd stress: 0.90 E_B//120 °C/24 h, the 3rd stress: 0.95 E_B/125 °C/24 h, the 4th stress: 0.95 E_B/150 °C/24 h.

The leakage current was recorded at intervals of 1 min during applying the stress using a high voltage source-measure unit (Keithley 237). The degradation rate coefficient (K_T) was calculated from the following expression: $I_L=I_{Lo}+K_T\ t^{1/2}$, where I_L is the leakage current at stress time (t), and I_{Lo} is I_L at $t=0$ [21]. After applying the respective stress, the E–J characteristics were measured at room temperature.

3. Results and discussion

Fig. 1 shows the SEM micrographs of the samples for different amount of Y_2O_3. On the whole, the grains of the samples were uniformly distributed and one of the features of surface morphology is some little porosity. It was obvious that the porosity decreased with an increase in the amount of Y_2O_3. All the samples revealed the presence of Pr-rich (Pr_6O_{11} and Pr_2O_3) and Y-rich intergranular layer (whitish bulk) as minor secondary phases, in addition to major phase of ZnO (blackish) by the XRD patterns as indicated in Fig. 2, whereas no La-rich phase was detected within detection limit of XRD. As a result, this system shows simple microstructure consisted of only major phase and intergranular layer [4,6–8], unlike multi-phases in ZnO–Bi_2O_3-based varistor ceramics. As the amount of Y_2O_3 increased, the densities (ρ) sintered pellets noticeably increased from 4.97, 5.18, and 5.20 g/cm^3 (5.78 g/cm^3 in pure ZnO), unlike Y_2O_3-doped 5-component-based ceramics, in which the ρ decreased with an increase in the amount of Y_2O_3. It is assumed that this is attributed to the effect of La_2O_3 in this composition. The average grain size (d) decreased from 4.1, 3.9, and 3.7 μm with an increase in the amount of Y_2O_3.

Fig. 3 shows the E–J characteristics of the samples for different amount of Y_2O_3. The E–J characteristics of varistors are divided into a nonconduction region and a conduction region. The varistors using these E–J characteristics can be applied as voltage switching devices. A knee-shape on the curves between the two regions indicates poor or better

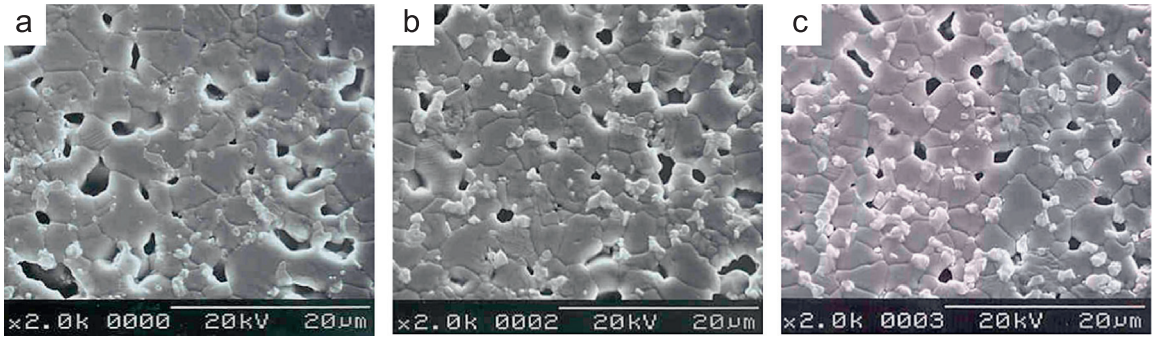

Fig. 1. SEM micrographs of the samples for different amount of Y_2O_3: (a) 0.25 mol%, (b) 0.5 mol%, and (c) 1.0 mol%.

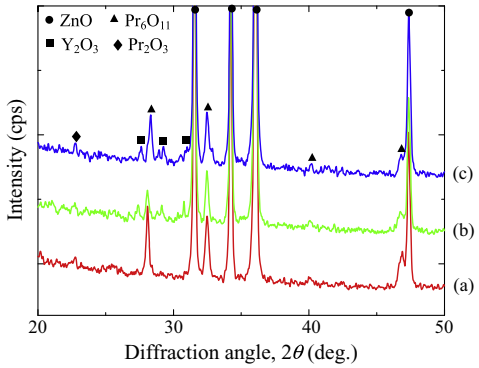

Fig. 2. XRD patterns of the samples for different amount of Y_2O_3: (a) 0.25 mol%, (b) 0.5 mol%, and (c) 1.0 mol%.

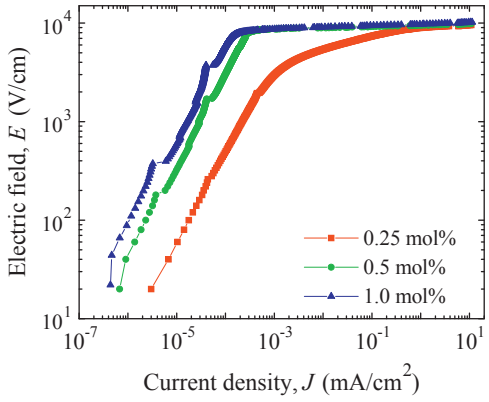

Fig. 3. *E–J* characteristics of the samples for different amount of Y_2O_3.

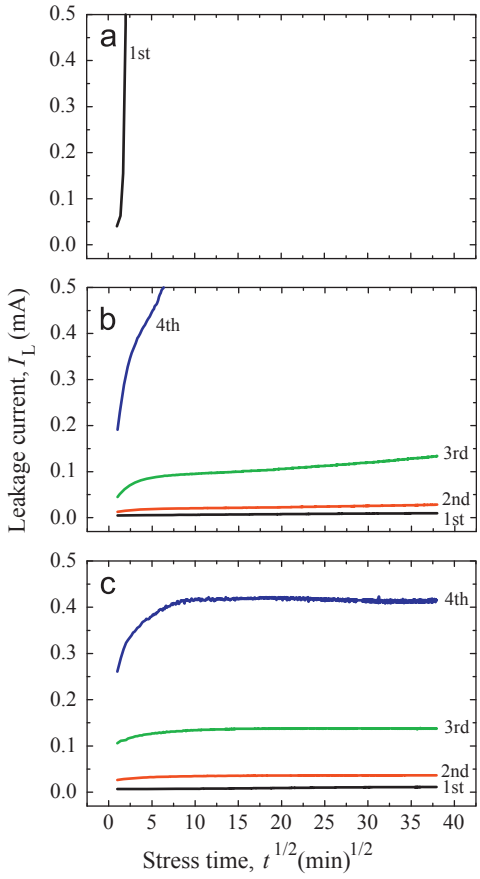

Fig. 4. Leakage current behavior during applying the stress of the samples for different amount of Y_2O_3: (a) 0.25 mol%, (b) 0.5 mol%, and (c) 1.0 mol%.

nonlinear properties. An increase in the amount of Y_2O_3 shifted the electric field curves to higher field strengths in the nonconduction region.

The breakdown field (E_B) greatly increased from 8953 to 9731 V/cm with an increase in the amount of Y_2O_3. The samples provided very high breakdown field per unit thickness (1 mm). Therefore, theses samples will be suitable for high voltage varistors with a compact size. The E_B depends on absolutely grain size. The increase of E_B with an increase in the amount of Y_2O_3 can be explained by the increase in the number of grain boundaries due to the decrease of average grain size as the following expression: $E_B = v_b/d$, where v_b is the breakdown voltage per grain boundary, and d is the average grain size. The v_b values of the samples were within the normal range of values of 2–4 V/gb.

The nonlinear coefficient (α) increased from 36.6 to 60.9 up to 0.5 mol% with an increase in the amount of Y_2O_3 and further increase caused α to decrease to 52.5 at 1.0 mol%. The maximum α was obtained from the sample doped with 0.5 mol% and this shows very high nonlinear properties. The α-behavior of ∧-shape in the amount of Y_2O_3 shows that the α sensitively depends on the amount of Y_2O_3. The behavior of α can be related to the Schottky barrier height, which induces from the electronic defect states at the grain boundaries. The amount of Y_2O_3 will vary the density of the interface states at grain boundary with the transport of the defect ions toward the grain boundary. The defect ions are oxygen, oxygen vacancies, zinc vacancies, etc. The J_L decreased from 79.6 to 0.16 μA/cm^2 with an increase in the amount of Y_2O_3. The samples doped with 0.5 and 1.0 mol% in the amount of Y_2O_3 exhibited extremely low leakage current of below 50 nA and these is truly unusual value, compared with other varistor ceramics. This result is one of important issues in this study. As a result, it was found that the appropriate amount of Y_2O_3 could improve the *E–J* characteristics; namely, it leads to high nonlinear coefficient and low leakage current. Obviously, the values of α and J_L were affected by the amount of Y_2O_3. The detailed electrical parameters are summarized as initial values in Table 1.

Fig. 4 shows the behavior of leakage current of the samples during various DC-accelerated aging stresses in accordance with the amount of Y_2O_3. The samples doped with 0.25 mol% in the amount of Y_2O_3 exhibited the thermal runaway at the first stress (0.85 E_B/115 °C/24 h). It is assumed that the thermal runaway of the samples is predominantly attributed to a low sintered density and high leakage current. A low sintered density decreases the number of conduction paths, and eventually leads to the concentration of current. Furthermore, a high leakage current leads to high joule heat loss. Therefore, the thermal runaway phenomenon of the samples doped with 0.25 mol% in the amount of Y_2O_3 is attributed to a low sintered density and a high leakage current as indicated in Table 1. The sample doped with 0.5 mol% in the amount of Y_2O_3 exhibited high stability until the third stress (0.95 E_B/125 °C/24 h),

Table 1
E–J characteristic parameters before and after DC-accelerated aging stress for the samples for different amounts of Y_2O_3.

Y_2O_3 amount (mol%)	Stress state	K_T ($\mu A \cdot h^{-1/2}$)	E_B (V/cm)	$\%\Delta E_B$	α	$\%\Delta\alpha$	J_L ($\mu A/cm^2$)	$\%\Delta J_L$
0.25	Initial	–	8953	0	36.6	0	79.6	0
	1st	Thermal runaway						
0.5	Initial	–	9490	0	60.9	0	0.26	0
	1st	0.9	9482	−0.1	59.5	–2.3	3.1	1092.3
	2nd	2.2	9453	−0.4	51.6	–15.3	8.2	3053.8
	3rd	11.0	9402	−0.9	47.7	–21.7	14.8	5592.3
	4th	Thermal runaway						
1.0	Initial	–	9731	0	52.5	0	0.16	0
	1st	1.1	9734	0.0	51.9	–1.1	4.6	2775.0
	2nd	0.3	9728	0.0	51.7	–1.5	11.7	7212.5
	3rd	0.4	9729	0.0	52.7	0.4	17.3	10712.5
	4th	−2.3	9680	−0.5	51.2	–2.5	9.9	6087.5

whereas it causes thermal runaway at the fourth stress (0.95 E_B/150 °C/24 h). This result is attributed to a comparatively high sintered density and much lower leakage current, compared with the sample doped with 0.25 mol% in the amount of Y_2O_3. The sample doped with 1.0 mol% in the amount of Y_2O_3 exhibited very strong stability, with low leakage current of roughly 0.15 mA at the third stress (0.9 E_B/150 °C/24 h) and without thermal runaway with low leakage current of roughly 0.4 mA at the fourth stress (0.95 E_B/150 °C/24 h). This is excellent. The stability against a stress in the varistors can be estimated by the degradation rate coefficient (K_T), which indirectly indicates the degree of aging. This exhibits the slope of the leakage current for the stress time, as mentioned previously. In general, the lower K_T values, the higher stability. The behavior of K_T shows a parabolic curve for the samples doped with 0.5 mol% in the amount of Y_2O_3 and gradually downward curve in the samples doped with 1.0 mol% in the amount of Y_2O_3. The K_T of each sample reaches 11 $\mu A \cdot h^{-1/2}$ for the sample doped with 0.5 mol% in the amount of Y_2O_3 and only 0.4 $\mu A \cdot h^{-1/2}$ for the sample doped with 1.0 mol% in the amount of Y_2O_3 at the 3rd stress (0.95 E_B/125 °C/24 h). Furthermore, the sample doped with 1.0 mol% exhibited $K_T = -2.3$ $\mu A \cdot h^{-1/2}$ even after applying the fourth stress (0.95 E_B/150 °C/24 h). Table 1 summarizes the *E–J* characteristic parameters, such as the variation rates of the breakdown field ($\%\Delta E_B$), nonlinear coefficient ($\%\Delta\alpha$), and leakage current ($\%\Delta J_L$) after applying the DC-accelerated aging stress. The sample doped with 1.0 mol% in the amount of Y_2O_3 exhibited extremely low characteristic variation of 0% in $\%\Delta E_B$ and 0.5% in $\%\Delta\alpha$, respectively, after applying the third stress (0.95 E_B/125 °C/24 h). Furthermore, this sample exhibited extremely very low variation of −0.5% in $\%\Delta E_B$ and −2.5% in $\%\Delta\alpha$ even after applying the fourth stress (0.95 E_B/150 °C/24 h). This shows much higher stability than any other ZnO–Pr_6O_{11}–based varistors [8,13,16] as well as the samples without La_2O_3 or Y_2O_3 reported previously [11,12,14,15]. In particular, this sample exhibited excellent stability comparable with ZnO–Pr_6O_{11}–CoO–Cr_2O_3–Y_2O_3–Er_2O_3 ceramics [19], which exhibited highest stability of ZnO–Pr_6O_{11}-based varistors reported until now, despite high breakdown field and nonlinear coefficient. Conclusively, Y_2O_3-doping has a significant effect on varistor properties and stability against DC stress of the ZnO–Pr_6O_{11}–CoO–Cr_2O_3–La_2O_3 varistor ceramics.

4. Conclusions

Y_2O_3–doping effect on microstructure, electrical properties, and aging behavior of the ZnO–Pr_6O_{11}–CoO–Cr_2O_3–La_2O_3 varistor ceramics has been investigated. Microstructually, the sintered densities increased and the average grain size decreased with an increase in the amount of Y_2O_3. The increase in the amount of Y_2O_3 increased the breakdown field due to the decrease in the average grain size. The maximum value in the nonlinear coefficient was obtained at 0.5 mol% in the amount of Y_2O_3. However, the varistor ceramics doped with 1.0 mol% exhibited the highest stability under specified accelerated aging stress state. Conclusively, it can be seen that the nonlinear properties and stability of the ZnO–Pr_6O_{11}–CoO–Cr_2O_3–La_2O_3 varistor ceramics can be controlled by Y_2O_3 doping.

References

[1] L.M. Levinson, H.R. Pilipp, Zinc oxide varistor–a review, American Ceramic Society Bulletin 65 (1986) 639–646.
[2] T.K. Gupta, Application of zinc oxide varistor, Journal of the American Ceramic Society 73 (1990) 1817–1840.
[3] Y.-S. Lee, T.-Y. Tseng, Phase identification and electrical properties in ZnO-glass varistors, Journal of the American Ceramic Society 75 (1992) 1636–1640.
[4] K. Mukae, Zinc oxide varistors with praseodymium oxide, American Ceramic Society Bulletin 66 (1987) 1329–1331.
[5] K. Mukae, K. Tsuda, S. Shiga, Zinc oxide–praseodymium oxide elements for surge arresters, IEEE Transactions on Power Delivery 3 (1988) 591–598.
[6] A.B. Alles, R. Puskas, G. Callahan, V.L. Burdick, Compositional effect on the liquid-phase sintering of praseodymium oxides-based ZnO varistors, Journal of the American Ceramic Society 76 (1993) 2098–2102.
[7] Y.-S. Lee, K.-S. Liao, T.-Y. Tseng, Microstructure and crystal phases of praseodymium in zinc oxides varistor ceramics, Journal of the American Ceramic Society 79 (1996) 2379–2384.

[8] C.-W. Nahm, The nonlinear properties and stability of ZnO–Pr_6O_{11}–CoO–Cr_2O_3–Er_2O_3 ceramic varistors, Materials Letters 47 (2001) 182–187.
[9] H. Heng, X. Fu, Z. Fu, C. Wang, L. Qi, H. Miao, Effect of TiO_2 doping on microstructure and electrical properties of ZnO–Pr_6O_{11}–based varistor ceramics, Journal of Alloys and Compounds 497 (2010) 304–307.
[10] Z. Peng, X. Fu, Y. Zang, Z. Fu, C. Wang, L. Qi, H. Miao, Influence of Fe_2O_3 doping on microstructure and electrical properties of ZnO–Pr_6O_{11}–based varistor ceramic materials, Journal of Alloys and Compounds 508 (2010) 494–499.
[11] C.-W. Nahm, B.C. Shin, Highly stable electrical properties of ZnO–Pr_6O_{11}–CoO–Cr_2O_3–Y_2O_3–based varistor ceramics, Materials Letters 57 (2003) 1322–1326.
[12] C.-W. Nahm, B.-C. Shin, B.H. Min, Microstructure and electrical properties of Y_2O_3–doped ZnO–Pr_6O_{11}–based varistor ceramics, Materials Chemistry of Physics 82 (2003) 157–164.
[13] C.-W. Nahm, J.-A. Park, B.-C. Shin, I.-S. Kim, Electrical properties and DC–accelerated aging behavior of ZnO–Pr_6O_{11}–CoO–Cr_2O_3–Dy_2O_3–based varistor ceramics, Ceramics International 30 (2004) 1009–1016.
[14] C.-W. Nahm, Electrical properties and stability against dc accelerated aging stress of lanthania doped praseodymia-based zinc oxide varistor ceramics, Journal of Materials Science 41 (2006) 7272–7278.
[15] C.-W. Nahm, The effect of sintering temperature on electrical properties and accelerated aging behavior of PCCL-doped ZnO varistors, Materials Science and Engineering B 136 (2007) 134–139.
[16] C.-W. Nahm, Microstructure, electrical properties, and dc aging characteristics of Tb_4O_7–doped ZnO-based varistors, Journal of Materials Science 43 (2008) 2857–2864.
[17] C.-W. Nahm, Al doping effect on microstructure, electrical properties, aging behaviors of ZPCCY-based varistors, Journal of Materials Science: Materials Electronics 20 (2009) 718–726.
[18] C.-W. Nahm, Sintering temperature dependence of varistor properties and aging behavior in ZnO–Pr_6O_{11}–CoO–Cr_2O_3–Al_2O_3–Y_2O_3 ceramics, Journal of the American Ceramic Society 93 (2010) 2297–2304.
[19] C.-W. Nahm, Microstructure, electrical properties and aging behavior of ZnO–Pr_6O_{11}–CoO–Cr_2O_3–Y_2O_3–Er_2O_3 varistor ceramics, Ceramics International 37 (2011) 3049–3054.
[20] J.C. Wurst, J.A. Nelson, Lineal intercept technique for measuring grain size in two-phase polycrystalline ceramics, Journal of the American Ceramic Society 55 (1972) 109–111.
[21] J. Fan, R. Freer, Deep level transient spectroscopy of zinc oxide varistors doped with aluminum oxide and/or silver oxide, Journal of the American Ceramic Society 77 (1994) 2663–2668.